Trans Indian Inst Met (2022) 75(4):1051–1068
https://doi.org/10.1007/s12666-022-02559-9

ORIGINAL ARTICLE

Pathways to Titanium Martensite

Yufeng Zheng[1] · Rajarshi Banerjee[2] · Yunzhi Wang[3,4] · Hamish Fraser[3,4] · Dipankar Banerjee[5]

Received: 14 December 2021 / Accepted: 9 February 2022 / Published online: 26 March 2022

Abstract The structural relationship between the parent and product phases in the martensitic transformation from the parent β phase is described. The atomic movements leading to the martensite are accomplished by a long-range shear $\{112\} < 111 >$ that transforms the parent to the product lattice and a short-wavelength displacement or shuffle $\{110\} < 110 >$ that induces the correct stacking. The microstructures arising out of these paths depend on which of these modes initiates the transformation. When the shear precedes the shuffle, conventional martensite forms as dislocated laths or internally twinned plates. A signature of the $\{110\} < 110 >$ shuffle that follows or accompanies the shear is present in both cases as stacking fault-related domains. The shuffle displacement precedes the shear with increasing β stabilizer addition, resulting in a nanodispersion of a structure with orthorhombic symmetry, which we have designated as O′. Al, Sn, Zr and O additions promote the shuffle. The O′ dispersion acts as embryos for the formation of nanomartensite on cooling or with the application of stress. The resulting continuous and controlled strain incorporation into the lattice within the constrained nanoembryos results in nonlinear superelasticity or the invar and elinvar effects. The stability of the bcc parent is discussed in terms of phonon mode or related elastic constant softening.

Keywords Titanium alloys · Martensite · High-resolution electron microscopy

1 Introduction

Srikumar Banerjee and Pradip Mukhopadhyay in a classic book on phase transformations [1] describe rigorously the thermodynamics and phenomenological crystallographic theory of martensitic transformations applied to titanium and zirconium alloys. Titanium has two allotropic modifications: the high-temperature bcc phase (Im3m, designated β) and the low-temperature hcp phase ($P6_3mcm$ designated α). A typical phase diagram of Ti with alloying additions that stabilize the β phase (usually a bcc metal) is shown in Fig. 1. Quenching from the β phase results in the formation of martensite with an hcp structure (α′) that is identical to that of the equilibrium α phase at low levels of alloying addition, or an orthorhombic martensite (α″, with a space group Cmcm) which is closely structurally related to α′ with increasing β stabilizer addition. Two other metastable phases, O′ and ω, are observed on quenching. We will describe the relationship between α′, α″ and O′ in describing the pathways to martensite formation.

The Bain path introduces the concept of a homogeneous lattice strain that can transform a parent to product martensite. The lattice correspondence usually chosen between the parent and product involves the minimum Bain strain. An appropriate lattice correspondence between

✉ Dipankar Banerjee
dbanerjee@iisc.ac.in

[1] Department of Chemical and Materials Engineering, University of Nevada Reno, Reno, NV, USA

[2] Materials Research Facility and Department of Materials Science and Engineering, University of North Texas, Denton, TX, USA

[3] Department of Materials Science and Engineering, The Ohio State University, Columbus, OH, USA

[4] Center for the Accelerated Maturation of Materials (CAMM), The Ohio State University, Columbus, OH, USA

[5] Department of Materials Engineering, Indian Institute of Science, Bangalore, India

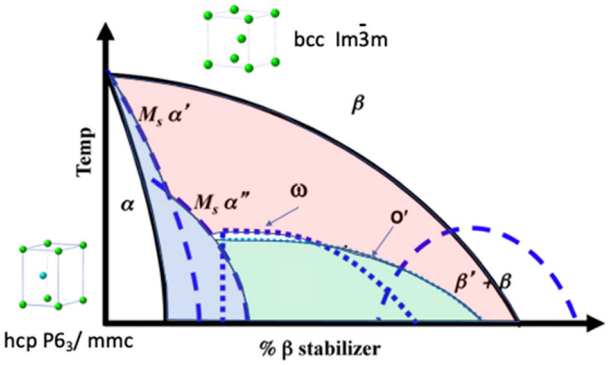

Fig. 1 The phase diagram of a typical titanium alloy with β stabilizer additions. The start temperatures of athermal metastable martensitic, ω, O′ and phase separation reactions are indicated

the bcc and hcp structures was first described by Burgers in 1934 [2]. The relationship between the two structures is best visualized by examining the projected atomic distribution along the [0001] direction of the hcp phase and the $< 110 >$ direction of the bcc phase, as in Fig. 2 [3]. In both cases, the structure can be described by an ABAB stacking along the projection direction. The phenomenological theory of martensitic transformations describes the transformation in terms of a Bain strain that converts the inscribed orthorhombic unit cell in a group of 4 bcc unit cells in Fig. 3 to the hcp lattice. The principal axes of strain are shown in Fig. 3 in a projected representation. A small rotation that places the $< 11\ \bar{2}\ 0 >$ direction parallel to either one of the two $< 111 >$ directions in the $\{110\}$ plane results in an undistorted and unrotated habit plane, as required by the phenomenological theory. An additional atomic shuffle completes the structural change and is described next.

An alternative way to visualize the transformation is to invoke a simple shear close to either of the two possible $\{112\} < 111 >$ shear systems associated with a given $\{110\}$ plane, one of which is shown in Fig. 4a. This shear combines the Bain strain and a rigid body rotation described in Fig. 3. An additional shuffle of the atoms in the B layer of the bcc structure is required to obtain the geometry of the ABAB stacking of the hcp phase. This shuffle can occur in either the positive or negative $< 110 >$ direction in the $\{110\}$ plane as shown in Fig. 4b, which must be examined in conjunction with Fig. 2. The orientation relationship between β and α that results from the lattice correspondence described above is (110) β // (0001) α′; [1 $\bar{1}$ 1] β // [11 $\bar{2}$ 0] α′. This is known as the Burgers orientation relationship (BOR) and leads to 12 rotational variants of the martensite. The alternative directions for the shuffle lead to two translational variants within each rotational variant, as shown in Fig. 4b. Figure 5 shows that the orthorhombic martensite, α″, present in β enriched alloys (Fig. 1) can be understood based on an incomplete shear/Bain strain such that the angle between the $< 111 >$ directions does not go to 60° but an intermediate value that

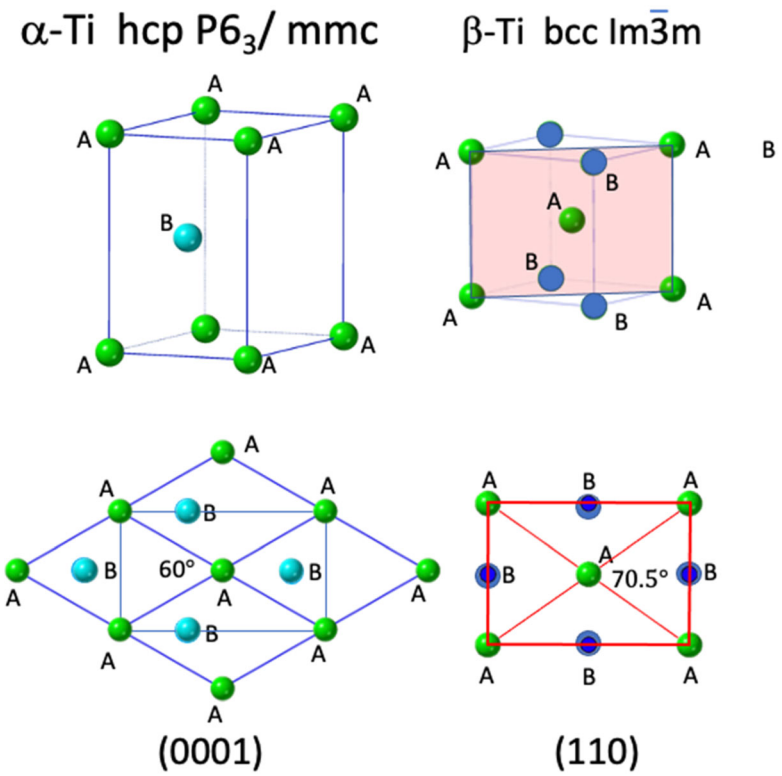

Fig. 2 The relationship between the β and α structures illustrated in isometric views and projected atom positions on the (0001) α and (110) β planes

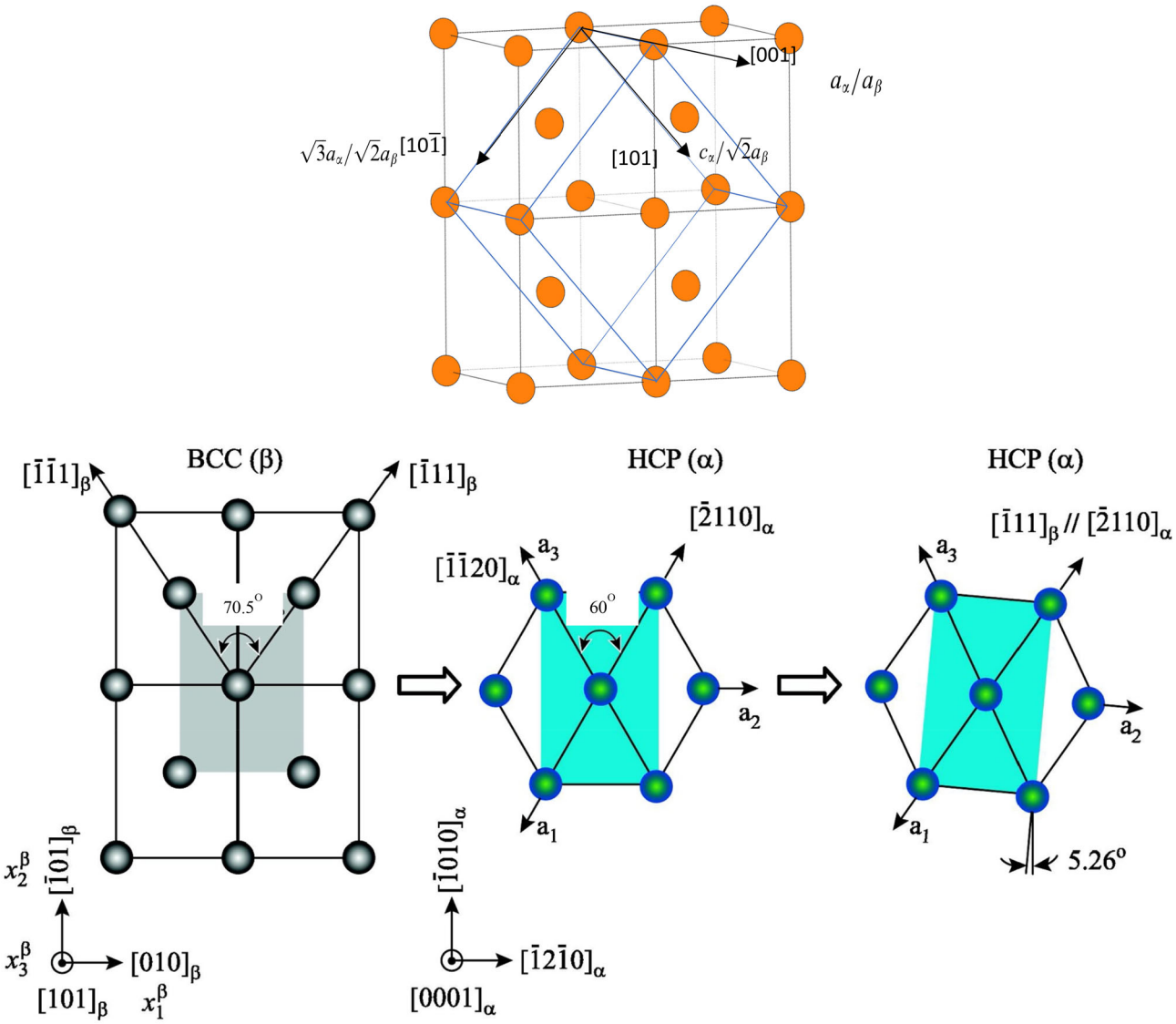

$$F_0 = \begin{bmatrix} a_\alpha/a_\beta & 0 & 0 \\ 0 & \sqrt{3}a_\alpha/\sqrt{2}a_\beta & 0 \\ 0 & 0 & c_\alpha/\sqrt{2}a_\beta \end{bmatrix} \quad F_R = \begin{bmatrix} \cos(5.26^\circ) & -\sin(5.26^\circ) & \\ \sin(5.26^\circ) & \cos(5.26^\circ) & \\ & & 1 \end{bmatrix}$$

Fig. 3 An inscribed orthorhombic unit cell in a bcc lattice. The Bain strain (F_0) and rigid body rotation (F_R) are described with a [101] β projection (from Shi et al. [3]), along with the transformation strain matrices, F_0 and F_R, that relate the product α′ to the parent β in terms of the lattice parameters

varies with β stabilizer content. The extent of the shuffle, marked by the distance 'x' in the figure, can also vary with β stabilizer content for the transition to α″, but is necessarily fixed for the hexagonal martensite, α′. Thus, the orthorhombic martensite, α″, represents an intermediate structure between the parent β and α′, hcp martensite. This structure has a Cmcm symmetry with an orientation relationship with the parent β that can be described as (110) β // (001) α″ and [1 $\bar{1}$ 1] β // [1 $\bar{1}$ 0] α″.

Starting with the parent β in Fig. 6a, Fig. 6b and c emphasize that the transition to α′ (or α″) can proceed through two alternative pathways, one in which the shear precedes the shuffle (Fig. 6b) and the other in which the shuffle precedes the shear (Fig. 6c), both paths leading to

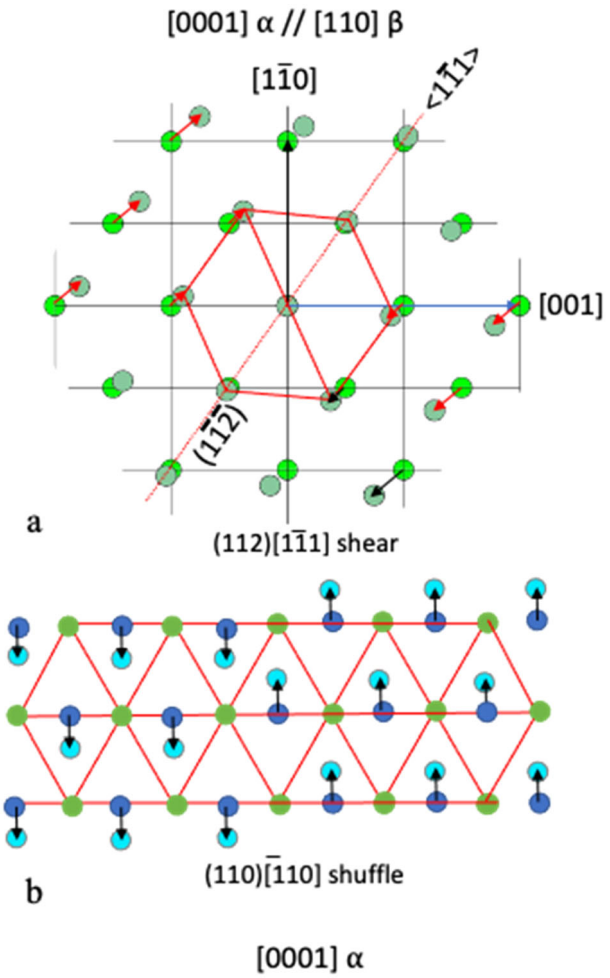

Fig. 4 The transformation from β to α described in terms **a** of a{112} < 111 > shear and **b** a (110) [1 $\bar{1}$ 0] shuffle

the final product, α′ (or α″) (Fig. 6d). Figure 6 also shows the alternative displacements leading to ω phase formation (Fig. 6e, discussed in detail in [1]). We have developed a greater understanding of these pathways in titanium alloys in recent years. We now describe the microstructures that arise from the choice of path and related properties.

2 The Effect of Composition on Pathways to Martensite

Banerjee and Mukhopadhyay [1] summarize the effect of β stabilizer addition on the Ms temperature, as shown in Fig. 7a. Thermodynamically, β stabilizer additions decrease the To temperature with increasing alloying content, and the Ms temperature would follow a similar trend with some degree of supercooling. Alloying additions which stabilize the α phase would increase the To temperature and therefore should increase the Ms temperature. Surprisingly, O, Al, Sn and Zr are believed to suppress the Ms temperature in alloys containing β stabilizer additions [4–7]. Indeed, it has been suggested that these alloying additions act as β stabilizers in highly alloyed titanium. Figure 7b provides examples of the suppression of Ms by some of these alloying additions. The very strong O effect indicates that data on Ms must be interpreted with due regard to the O content of the alloys being investigated. Our studies on pathways to the martensitic transformation in titanium alloys were initially provoked by this anomalous effect of α stabilizers such as Al and O.

The crystallography, the nature of lattice invariant deformation, morphology and distribution of martensite are described in detail in [1] from the perspective of the phenomenological theory. A transition from lath martensite with slip as the mode of lattice invariant deformation to twinned martensite occurs with increasing β stabilizer content. Irrespective of the mode of lattice invariant deformation, a fine substructure is found in both lath and twinned martensite and was recorded by Erickson et al. [8], Hammond and Kelly [9] and Knowles and Smith [10, 11] in Ti–Mn and Ti–Cr binary alloys. This substructure has been described in detail and analysed by Banerjee, Muraleedharan and Strudel [12] and is shown in Fig. 8. It manifests itself as striations in twins and untwinned regions at low magnifications. At higher magnifications and in suitable orientations and 2-beam conditions, the substructure resolves itself as an elongated domain structure, quite reminiscent of antiphase boundaries in ordered structures. However, contrast analysis shows that the displacement vector associated with these domain boundaries is 1/3 < 10 $\bar{1}$ 0 > or 1/3 < 20 $\bar{2}$ 3 > . These domains are associated with the (110)[1 $\bar{1}$ 0] shuffle described in Fig. 4, one of the two steps required to transform the parent β to α. As shown in Fig. 4d, the shuffle can occur in a positive or negative direction within a martensite plate leading to adjacent domains related by a translation shown in Fig. 8b, c to be 1/3 < 20 $\bar{2}$ 3 > . Figure 8b, e shows the domain shape in relation to the martensite plate and indicates that domains grow outward from the midrib of the martensite as the product interface migrates into the parent. While the macroscopic aspects of the transformation structure as derived from the phenomenological theory of martensite are consistent with the formulation of the Bain strain derived from the Burgers mode. The observation of the domain structure appears to be the first conclusive evidence that the martensitic transformation does proceed along the pathways defined by Burgers many years ago.

We now describe the effect of β stabilizer content on pathways to the martensite transformation, focusing on the anomalous effect of α stabilizer additions in depressing the Ms temperature. Tahara et al. [13], in examining β stabilized alloys containing a large amount of oxygen, described diffraction effects from the (110) [1 $\bar{1}$ 0] shuffle in the

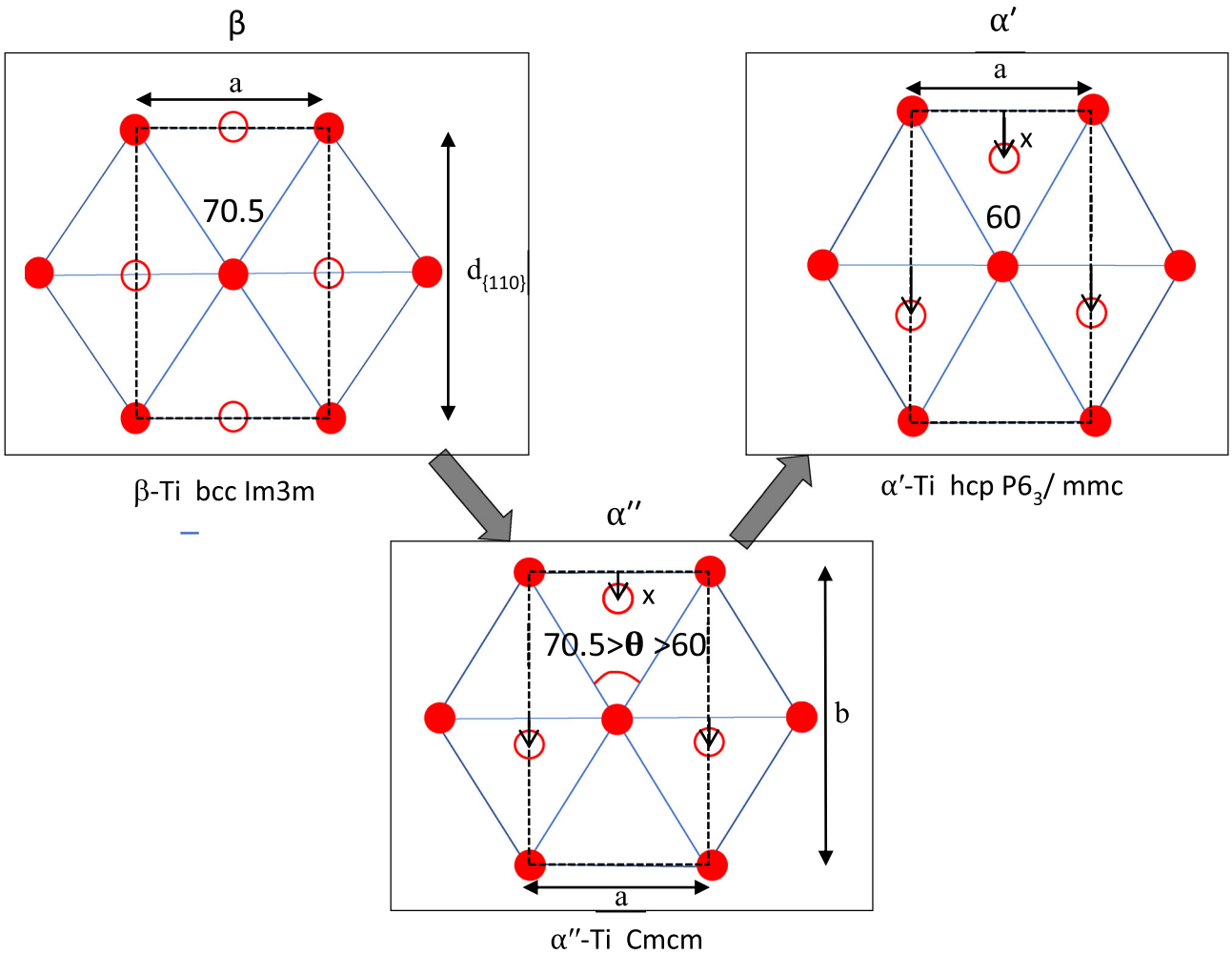

Fig. 5 The relationship between α′ (hcp) and α″ (orthorhombic) martensites

absence of the Bain strain and the associated existence of nanodomains. They pointed out that 12 variants of nanodomains can be formed with opposite shuffle directions for each of the six {110} planes, and the presence of these nanodomains can suppress the formation of martensite laths. We explored this effect in various compositions, binary Ti-Mo alloys, alloys in which Zr and Al were added to binary alloys of Ti–Nb and Ti–Mo, respectively, and finally extremely low oxygen-containing alloys [14–16]. Alloy compositions were chosen based on the Bo–Md diagram proposed by Abdel-Hady et al. [4] to describe the stability of the β phase. Thus, the binary compositions Ti–26Nb and Ti–9Mo lie adjacent to the β/β + ω boundary (compositions in atomic %). The addition of 2% Zr to a Ti–26Nb alloy and 9% Al to a Ti–9Mo change the location of the alloys on the Bo–Md diagram (Fig. 9) such that martensite would be expected to form on quenching the β phase. These additions, however, suppress the formation of martensite. We found that the nanodomain structure from the (110) [1 $\bar{1}$ 0] shuffle can occur in binary Ti-Mo alloys with increasing Mo additions (in the absence of martensite), that Al and Zr added to alloys containing high amounts of β stabilizer promote the formation of the nanodomain structure and that the shuffle-related transformation can also occur in extremely low oxygen alloys. We also found that the nanodomains can coexist with athermal ω.

Figure 10 shows diffraction from a quenched in β phase in Ti-12at%Mo. In the [110] zone axis, diffuse reflections occur at 1/3 {112} positions that arise from the ω phase. Additional diffuse reflections occur at ½{112} positions. In the [100] zone axis, diffuse reflections occur at ½{310} positions, shown by full arrows. Reflections at ½{110} positions can be shown to arise from double diffractions. A dark-field image from 1/2{310} reflections shows a nanodomain structure (Fig. 10c). We have simulated these diffraction effects, that is the ½{112} and ½ {310} reflections, with a structure with a Cmcm symmetry in

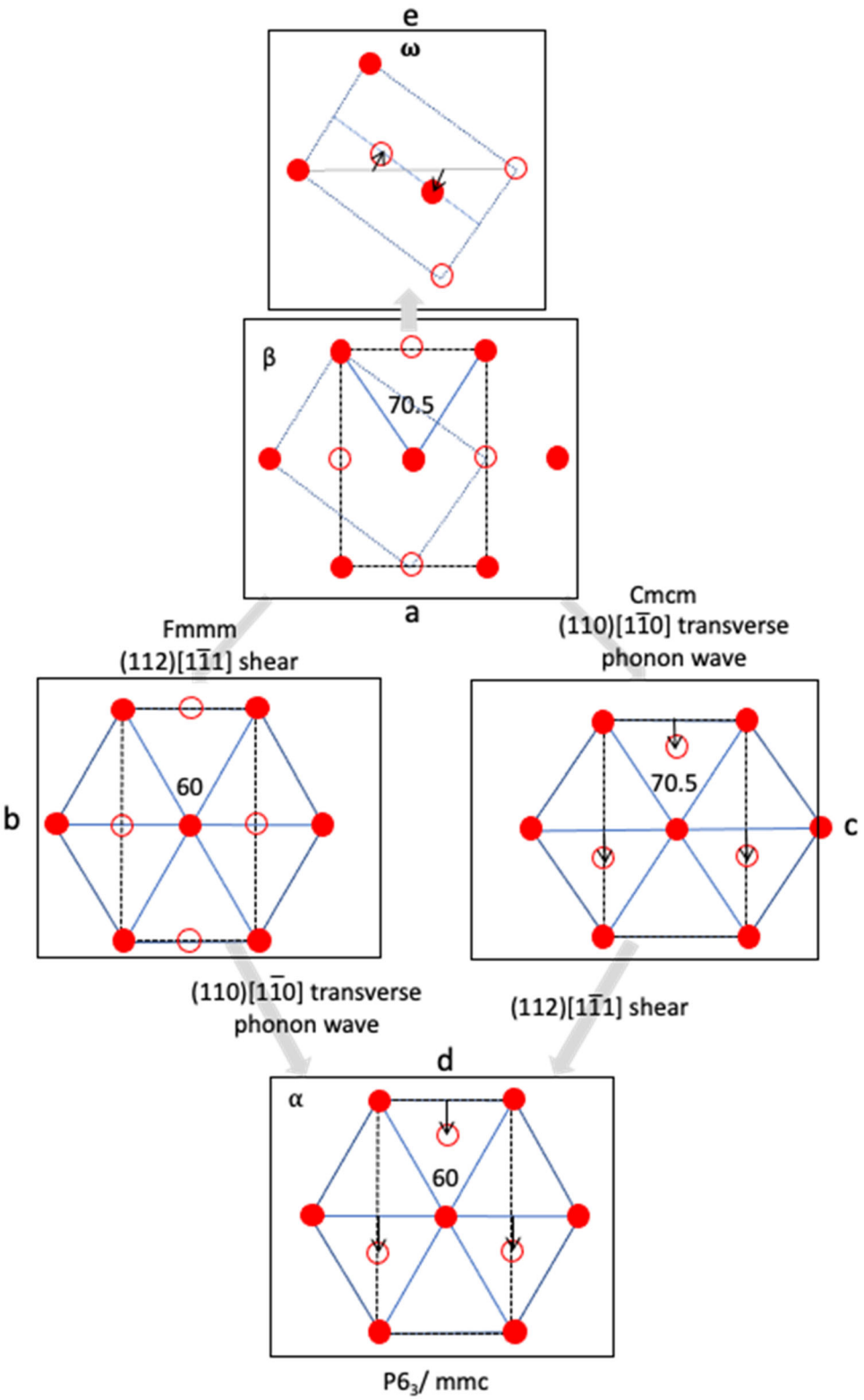

Fig. 6 **a**–c and **a**, **c**, **d** are alternative pathways to the α′ (hcp) / α″ (orthorhombic) martensites, and **e** displacements leading to ω for comparison

which the atoms on every alternate plane of the parent β phase are displaced by a small fraction along the [110] β direction consistent with the operation of the (110)[1 $\bar{1}$ 0] shuffle. The a-axis of this structure coincides with the a-axis of the β phase along the [001]β direction. The b and c-axes lie along two $< 110 >$ β directions perpendicular to the [001] direction. They are equal to $\sqrt{}$ 2a, such that no lattice distortion or dilatation of the β phase has been

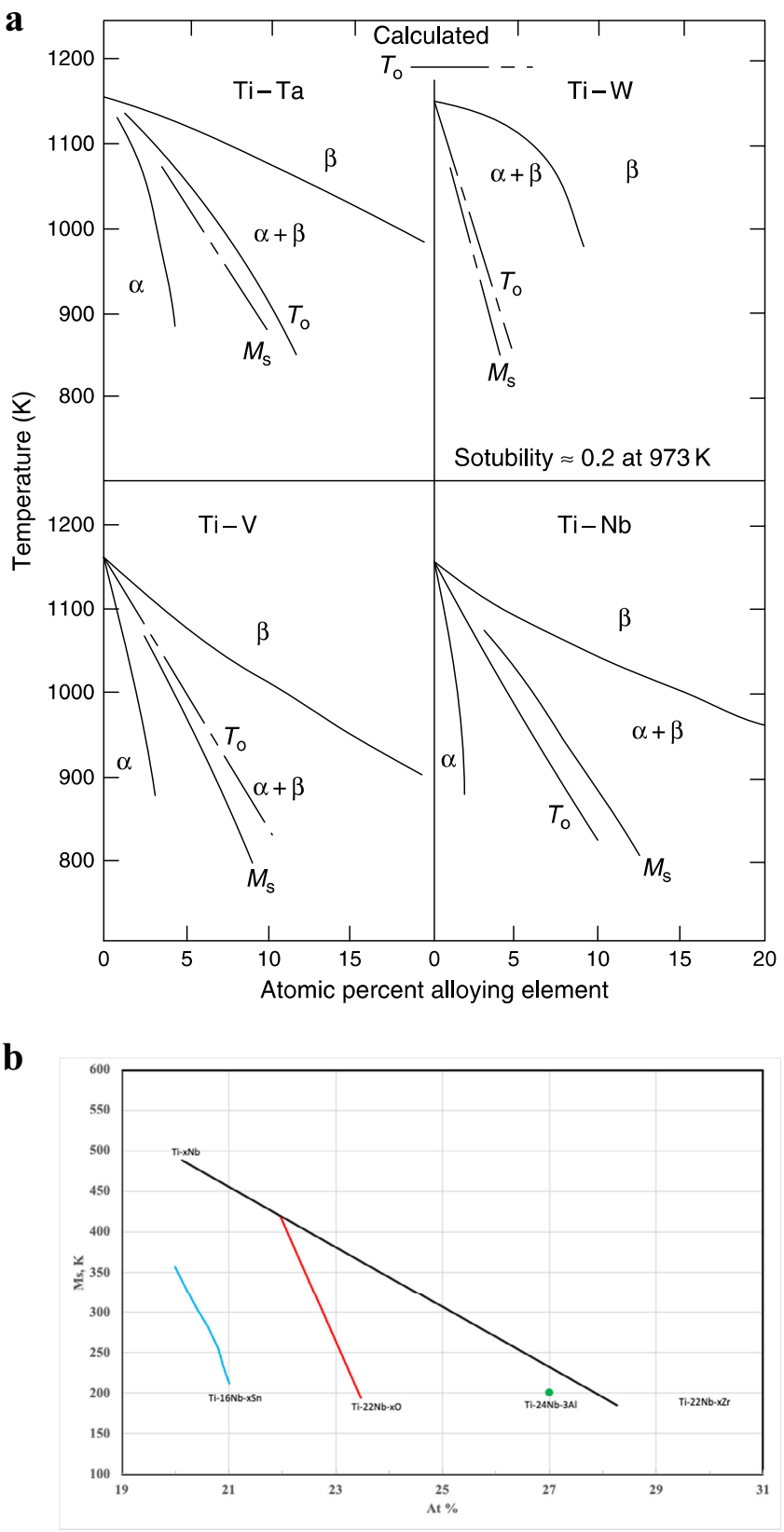

Fig. 7 **a** The effect of composition on the To and Ms temperature in titanium alloys with β stabilizer addition from Banerjee and Mukhopadhyay [1]. Surprisingly, Ms is shown as lying above To in the Ti–Nb system and might represent an error in calculation or plotting. **b** The effect of Sn, O and Al additions on the Ms temperature in alloys of the Ti–Nb system derived from references [5–7]

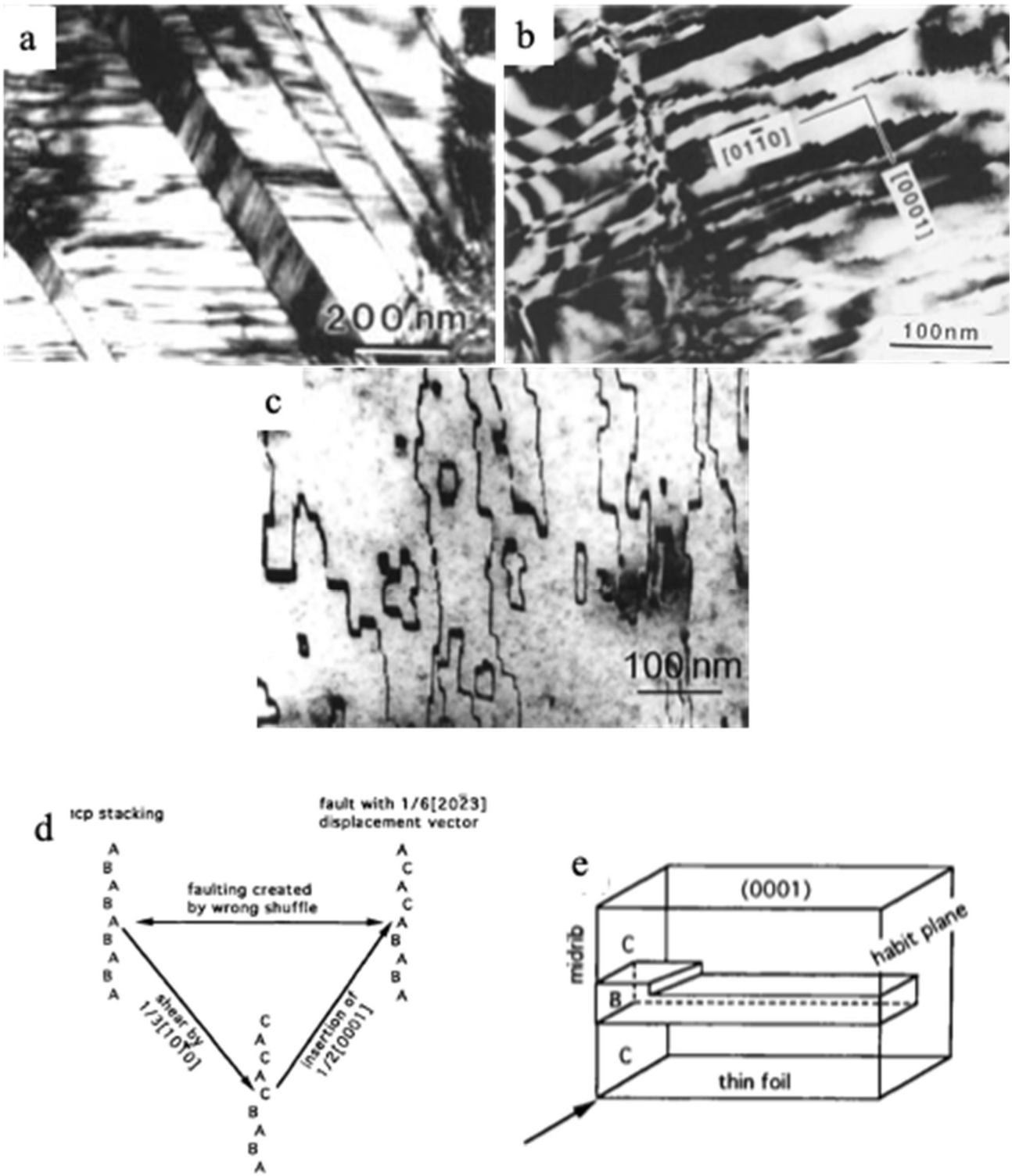

Fig. 8 **a** Striations within twins and matrix of martensite plates in an α + β titanium alloy, **b** domain structure extending out from the midrib of a martensite plate, **c** contrast from domain boundaries, **d** displacement vector associated with the domain boundaries, **e** morphology of the domain structure. All images from Banerjee et al. [12]

incorporated in the simulation. This simulation corresponds to the inscribed orthorhombic cell in the β phase shown in Fig. 3 but modified by the shuffle. The simulated patterns are also shown in Fig. 10. We have designated this phase as O′ to distinguish it from the equilibrium, ordered O phase in the Ti–Al–Nb system [17] and the ordered

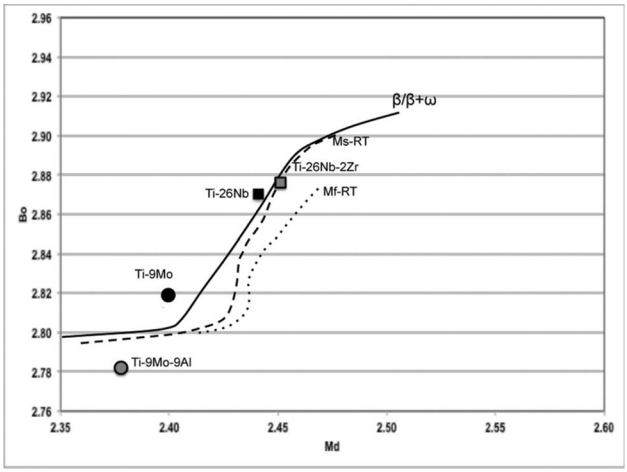

Fig. 9 The Bo–Md diagram for titanium alloys from Abdel-Hady et al. [4] with the compositions studied in [14] superimposed on the diagram

orthorhombic O″ phase that occurs on ageing in β -enriched alloys [18]. High-resolution STEM-HAADF imaging of the structure associated with such diffraction patterns shows the presence of both O′ and ω, as shown together with the displacements associated with each of the phases in Fig. 11 (see also Fig. 6). Figure 12 shows the effect of Al additions to a Ti–Nb alloy on the relative amounts of O′ and ω phases.

These results demonstrate that dilute alloys of titanium follow a path 'abd' in Fig. 6 in which the shear occurs first with a concurrent or following shuffle as the martensite interface grows into the parent. With increasing β stabilizer addition, and with Al, Sn, Zr or O additions, the shuffle occurs first (path 'acd' in Fig. 6) leading to completely coherent nanodomains of the O′. The immediate question is whether the transformation can be completed to martensite through path 'acd' in Fig. 6 if the temperature is decreased or equivalently due to increased stress at room temperature. We investigated this in a Ti–15Nb–2.5Zr–4Sn (at.%), designated Ti2448 from its composition in wt%, Ti–24Nb–4Zr–8Sn [19]. The reason for the choice of composition will be indicated later. The transition to martensite involves a measurement of the shuffle distance and the extent of shear either in direct or reciprocal space. The relevant measurements are shown in Fig. 13. The degree of shuffle can be measured as indicated in the figure. The degree of shear in the nanodomains at room temperature is evaluated by measuring the difference between the lattice parameter, $b_{O'}$, of the orthorhombic nanodomain (Fig. 13a) and interplanar spacing of $d_{\{110\}}$ in the bcc lattice (Fig. 13c). The normalized lattice strain $(b_{O'} - d_{\{110\}})/d_{\{110\}}$ is used to represent the amount of shear. These measurements are obtained by plotting intensity along the different dashed lines shown in the figure. For the O′ phase in this alloy at room temperature, $b_{O'}$ and $d_{\{110\}}$ are equal, indicating that only a shuffle has occurred. The degree of shuffle is only 4% of $d_{\{110\}}$, whereas a shuffle of 16.67% of $d_{\{110\}}$ is required for the transition from the bcc to hcp α′ phase. The nanodomains grow in size with decreasing temperature, as shown by in situ cooling in the TEM (Fig. 14a). Figure 14b shows that the normalized lattice strain increases concurrently, indicating a transition from the O′ to α″. The continuous increase in lattice strain suggests a second-order transition. The alloy has also been cold worked by 50% to evaluate the effect of stress on O′ domains. A transition to α″ occurs as shown in Fig. 15. The shear is apparent by following the solid red line from the β phase through α″ to β on the opposite side of the nano-α″. The behaviour may be contrasted with that of the solid red line in Fig. 12b.

We have thus demonstrated that transformation from parent β phase to martensite in titanium alloys can follow either of the two possible transition paths. The conventional, well-known path in dilute titanium alloys results in large martensite plates arising from the $\{112\} < 111 >$ shear, along with the concurrent or following shuffle within each plate, resulting in faulted domains within the martensite. The shuffle occurs first in β stabilizer enriched alloys but is also promoted by Al, O, Zr and Sn additions. This results in nanodomains of the O′ phase. Subsequent cooling or stress results in a continuous transformation of O′ nanodomains to nanodomains of α″ martensite.

3 On the Origin of Transition in Pathways to Martensite

Lattice stability is integral to our understanding of the pathways followed by the martensitic transformation. A solid in mechanical equilibrium is stable against small distortions, implying restrictions on the elastic constant values. The mechanical stability criterion for cubic systems is given by $C_{11} - C_{12} > 0$, $c_{11} + 2C_{12} > 0$ and $c_{44} > 0$. The origin of lattice instabilities in bcc or B2 parent phases has received attention primarily because of shape memory effects arising out of the martensitic transformation. The temperature dependence of elastic constants is closely related to the Burgers transformation mode [20]. While the Burgers model assumes that the $\{112\} < 111 >$ shear precedes the (110) [1 $\bar{1}$ 0] shuffle, it has been pointed out there is no reason to assume that this is so [21]. The elastic constant related to the $\{112\} < 111 >$ shear is shown to be [20]

$$Cs = C' + 1/2(C_{44} - C')\sin 2\theta s$$

where

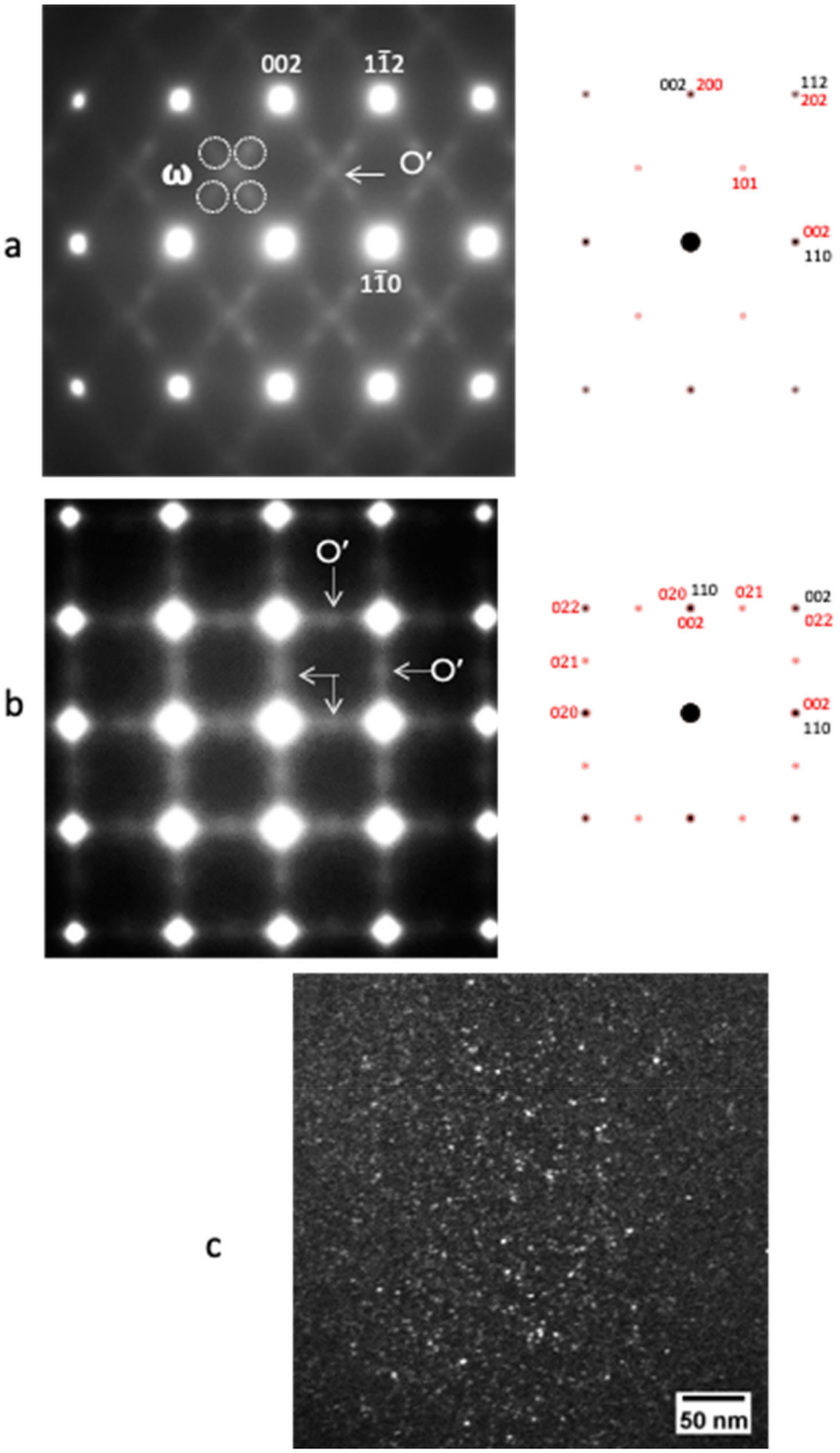

Fig. 10 **a** diffraction from the O′ and ω phases in a {110] β zone axis, **b** diffraction from O′ in [100] β zone axis. Two variants are present, and the arrows mark spots due to double diffraction. **c** Dark field using an O′ refection. Images from Zheng et al. [14–16]

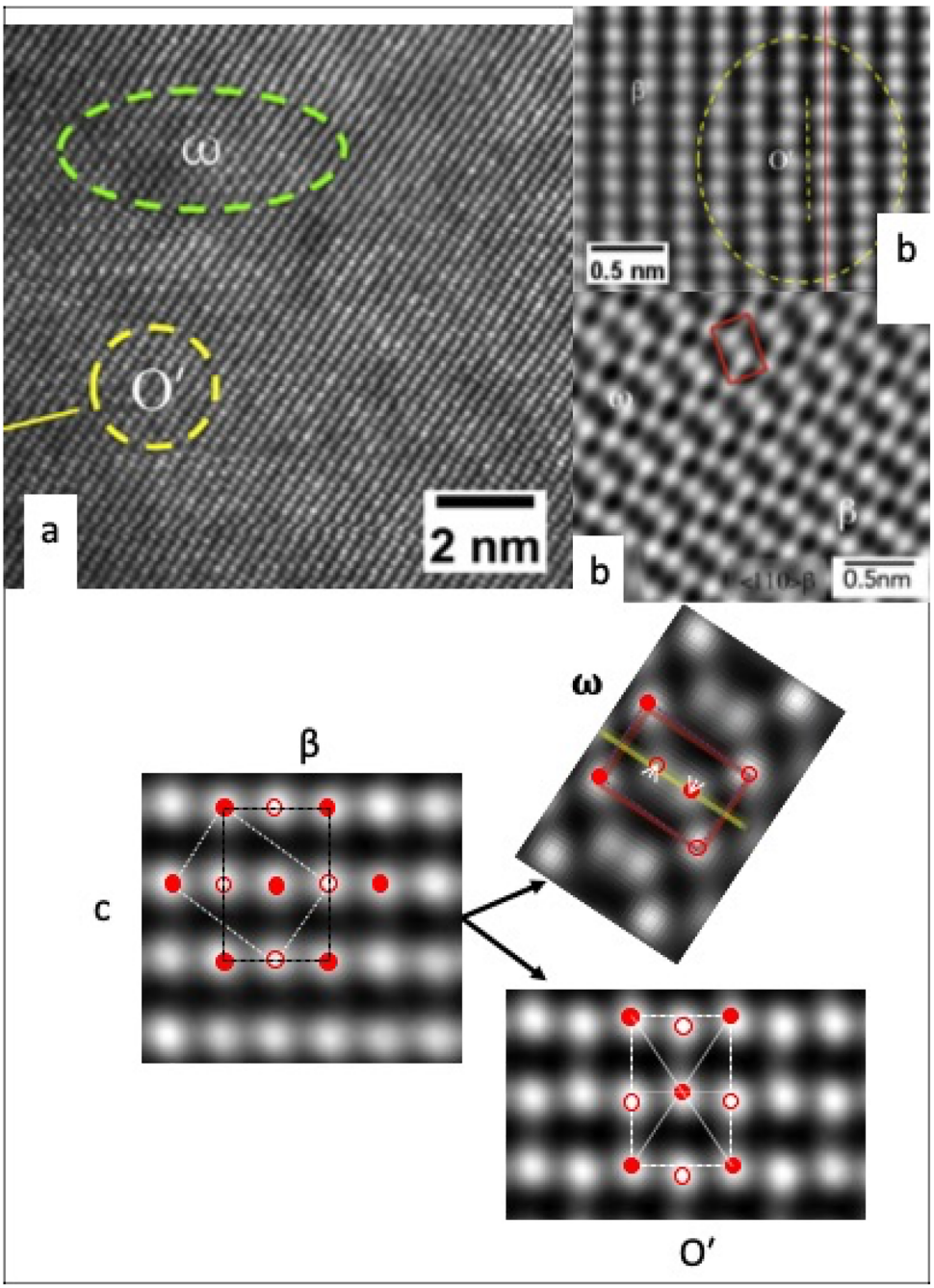

Fig. 11 **a** High-resolution HAADF images of the O′ and ω phase, **b** and **c** higher-magnification images from O′ and ω, respectively, with the displacements from β to O′ and ω marked with the associated unit cells superimposed in a [110] β zone axis. Images from Zheng et al. [15]

$$\theta s = \sin^{-1}[2(C_{11} + C_{12})/(3C_{11} + 5C_{12} + 2C_{44})]^{1/2}$$

while the elastic constant related to the (110)[1 $\bar{1}$ 0] shuffle is

$$C' = 1/2(C_{11} - C_{12}).$$

Which of these paths occurs first depends on the softening of these elastic constants as a function of temperature and whether Cs or C″ soften first as the temperature decreases. As an example of the softening, we show data for NiAl from Nakanishi et al. [20] in Fig. 16a, since similar data are not available at this time in titanium alloys. It has been suggested by Nakanishi et al. [20] that the softening of Cs results in an anharmonic coupling between C′ and C_{44} since nonlinearities in C′ and C_{44} occur at nearly the same temperature and precede softening of C′. However, it is clear from our work on titanium alloys that there must be a transition in the temperature dependence from softening of Cs and C′ such that the long-wavelength shear associated with a softening of Cs occurs first or simultaneously with the shuffle in dilute titanium alloys, while the softening of C′ precedes Cs in β enriched alloys, and that specific alloying additions can affect the

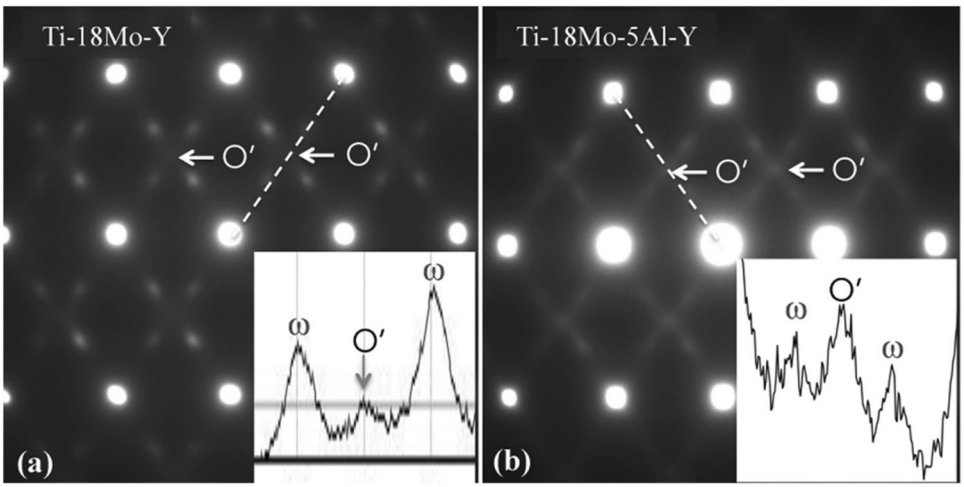

Fig. 12 The effect of Al addition on the relative amounts of O′ and ω phases in a Ti–Mo alloy with ultra-low oxygen content in the matrix, realized by Y additions. Images from Zheng et al. [16]

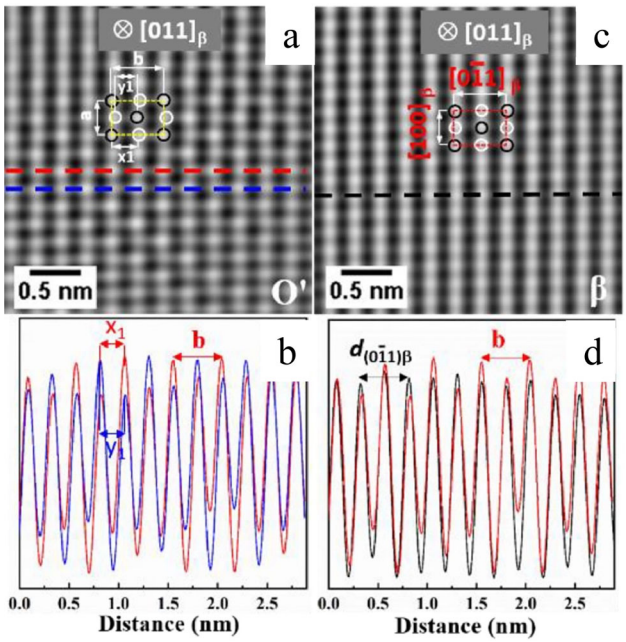

Fig. 13 **a** HAADF-STEM image acquired with the incident electron beam parallel to [0 1 1] β showing an orthorhombic nanodomain. The degree of shuffle can be obtained from the distance × 1-y1, **b** intensity profiles along the red and blue lines in **a** showing the displacement of every other (0 1 1) β, **c** HAADF-STEM image of the β matrix recorded with incident electron beam parallel to [0 1 1] β; **d** intensity profiles plotted along the black line in **c** and red line in **a** with direction of [0 1 $\bar{1}$]β, measuring the interplanar spacing difference between d(0 1 $\bar{1}$)$_\beta$ and $b_{O'}$. This difference is measure of the shear associated with the transition of O′ to α″. Images from Liang et al. [19] (color figure online)

temperature dependence. Therefore, we have schematically indicated the temperature at which softening of the relevant elastic constants occurs in Fig. 16b. This requires experimental/theoretical verification currently.

In an analogous description, dynamic distortions in a crystalline solid can be described in terms of phonons or normal modes of vibration [22]. A displacive transformation is associated with the anomalous behaviour of one of these modes. Figure 17b shows the behaviour of relevant phonon dispersion curves for titanium recorded in the stable β phase region at high temperature [23]. These phonon dispersion curves have been obtained along different reciprocal lattice vectors indicated on the first Brillouin zone of the bcc lattice in Fig. 17a. Anomalous softening is seen for phonons with the transverse wave vector $\vec{q} = \frac{1}{2}(110)$, $\vec{p} = [1\bar{1}0]$ and the longitudinal wave vector $\vec{q} = \frac{2}{3}(111)$, $\vec{p} = [111]$, where q and p are the wave number and polarization vectors, respectively. These are related to the displacements leading to the O′ and ω phase, respectively. Thus, the β phase has an inherent instability to these displacements well above any critical temperature. The long-wavelength shear $\{112\} < 111 >$ is defined by the slope of the TA curve at the origin of the Brillouin zone in this figure along the off-symmetry $\xi\xi 2\xi$ phonon branch. Similar phonon dispersion curves have been obtained in Ti–V alloys [24]. Table 1 lists these critical soft phonon wave numbers and related elastic constants for the β to O“, α″ and ω transformations. It has been pointed out that structural transformations based on phonon mode softening [22] must have a second-order character.

The O′ phase that arises from the (110) [1 $\bar{1}$ 0] shuffle is an example of a precursor state to the martensite. Such a precursor state has been likened to a strain glass (for a review see [25] or [26]) in a ferroelastic system, in analogy with other states that correspond to local order in a statistically disordered phase (Fig. 18) such as the structural glass state in liquid–solid transitions, or the cluster-spin transition in ferromagnetic systems and the relaxor (or local electric dipole ordering) transition in ferroelectric transitions. A strain glass state has been well characterized in the TiNi system. We suggest that the Landau free energy landscape associated with the O′ to α″ transformation is as

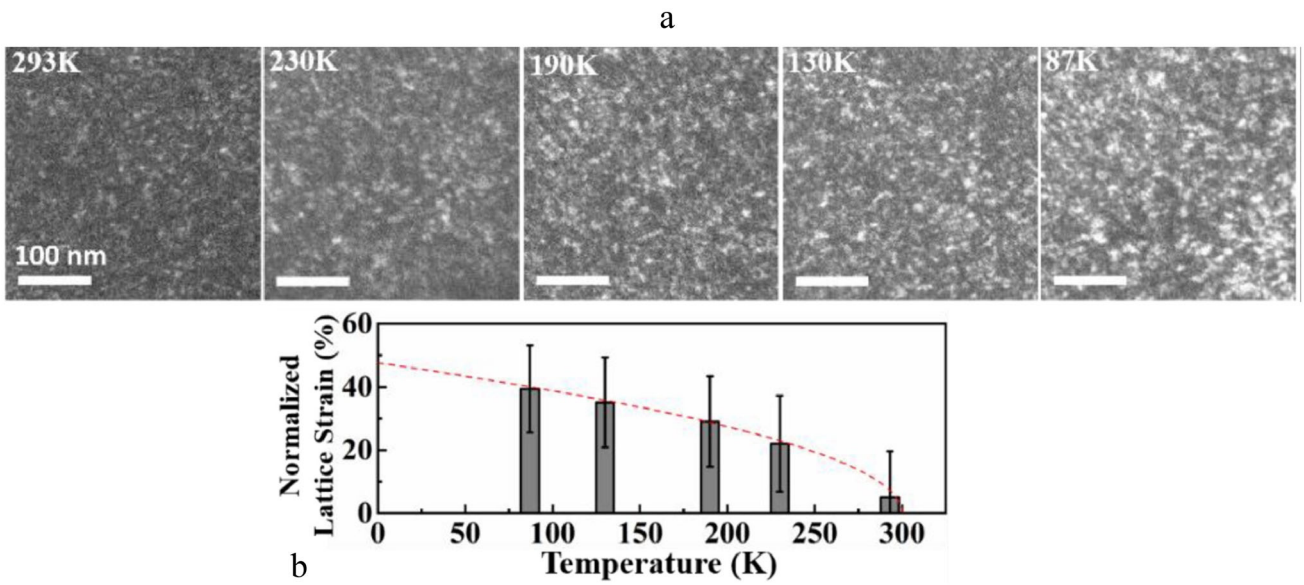

Fig. 14 **a** The effect of cooling on the growth of nanodomains, **b** the normalized lattice strain as a function of cooling. Images from Liang et al. [19]

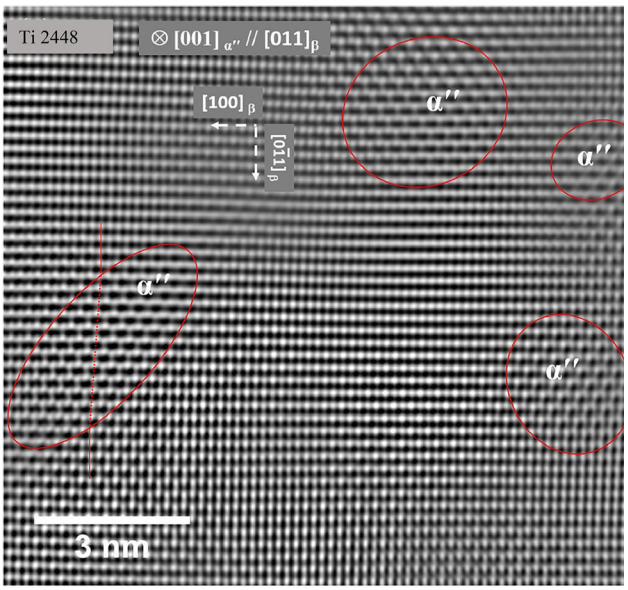

Fig. 15 The formation of nanodomains of α″ on cold working the Ti2448 alloy. Image from Liang et al. [19]

shown in Fig. 18, in contrast to that for β to α″ transformation, resulting in increasing lattice shear without an energy barrier.

4 Physical and Mechanical Behaviour

The martensitic transformation in titanium and its alloys was investigated in the seventies and eighties. However, this transformation is not utilized in conventional engineering alloys of titanium. The recent emergence of additive manufacturing with its associated rapid cooling rates has again sparked interest in the conventional martensite in relatively dilute engineering alloys of titanium. A recent summary of martensite and related mechanical behaviour of additively manufactured Ti6Al4V is provided in [27]. We briefly describe in this section the intriguing properties seen in multifunctional β titanium alloys of which gum metal, Ti–23Nb–0.7Ta–2Zr–O [28]and Ti2448 [29] are examples. Figure 19a shows an example of superelastic behaviour in the Ti2448 alloy with low hysteresis, and continuous softening with stress is shown in Fig. 19b. The latter behaviour is different from that observed in alloys which show stress-induced martensitic transformation in which typical stress–strain curves exhibit a stress plateau due to the abrupt martensitic transformation. In addition, superelastic behaviour is observed over an extended temperature range, unlike in conventional shape memory alloys (Fig. 19c). The thermal coefficient of expansion can be tuned by applied strain, as shown in Fig. 19d. The invar-like behaviour in gum metals is shown in Fig. 19e.

Normal martensitic transformations are sharp and non-linear due to autocatalysis and rapid, uncontrollable growth of martensitic plates with long-range strain after nucleation from a first-order reaction (Fig. 18). This leads to structural defects, large stress–strain or temperature–strain hysteresis and strongly nonlinear pseudo-elasticity, typical of classic shape memory alloys. If the discontinuous, first-order transformation could be modified in some manner to a gradual, continuous mode that occurs over a range of

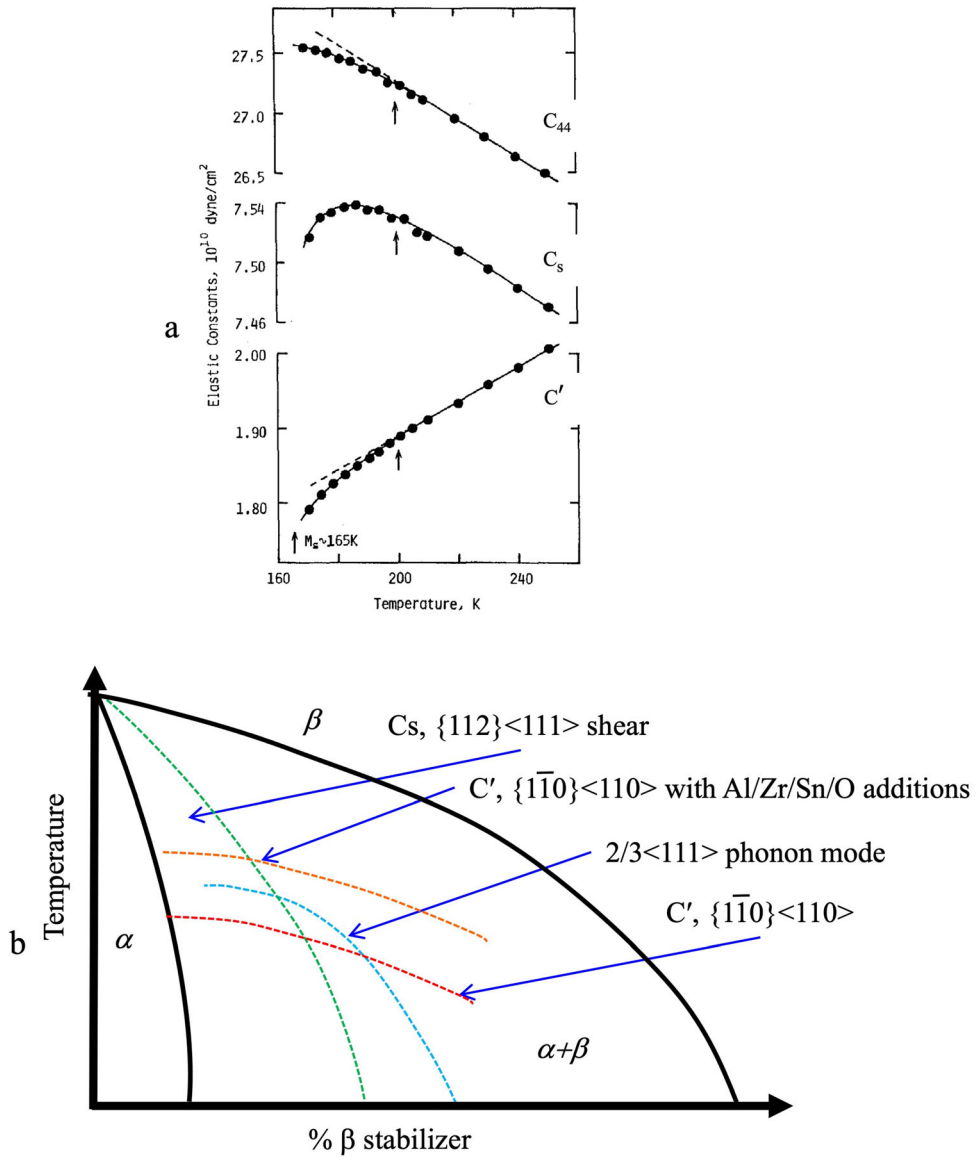

Fig. 16 **a** The softening of elastic constants relevant to the martensitic transformation in NiAl, from Nakanishi et al. [20], **b** the softening temperature of relevant shear constants as a function of β stabilizer content, shown schematically by the dashed lines [15]. The difference between the softening temperature of Cs and C′ has been exaggerated for clarity

temperature or stress, then new functional behaviour can emerge [29–31]. It has been shown that nanoscale concentration variations can alter the nature of the martensitic transformation in terms of spatio-temporal variations of martensite stability and transformation strain to realize continuous behaviour [32–35]. Creating a nanoscale precursor state to martensite is an alternative approach to realize a second-order type, continuous transition in which martensite is confined to nanodomains. This mechanism is distinct because, in the former approach, the long-range strain of martensite is retained but the concentration modulation defines the phase stability and thus the physical boundaries of the martensite product. In the latter case, the embryos associated with the precursor state lead to the nanoscale martensitic product.

While detailed descriptions of the invar, elinvar and nonlinear superelasticity effects arising out of confined, continuous growth of nanodomains of martensite are available [30–32], we qualitatively describe here the basis of the observed behaviour. The transformation pathway of O′ to α″ results in continuously increasing shear components within α″ at the nanoscale on cooling due to the local constraint caused by O′ nanodomains. The resultant softening of the elastic modulus during cooling compensates normal modulus hardening in the bcc lattice, leading to the elinvar effect. Similarly, the transformation strains during cooling can compensate for the normal lattice contraction leading to the invar effect. Cold work offers additional control over the nanostructure in that O′ domains transform during cold work to nanodomains of α″. These nanodomains can reorient under subsequent stress leading to

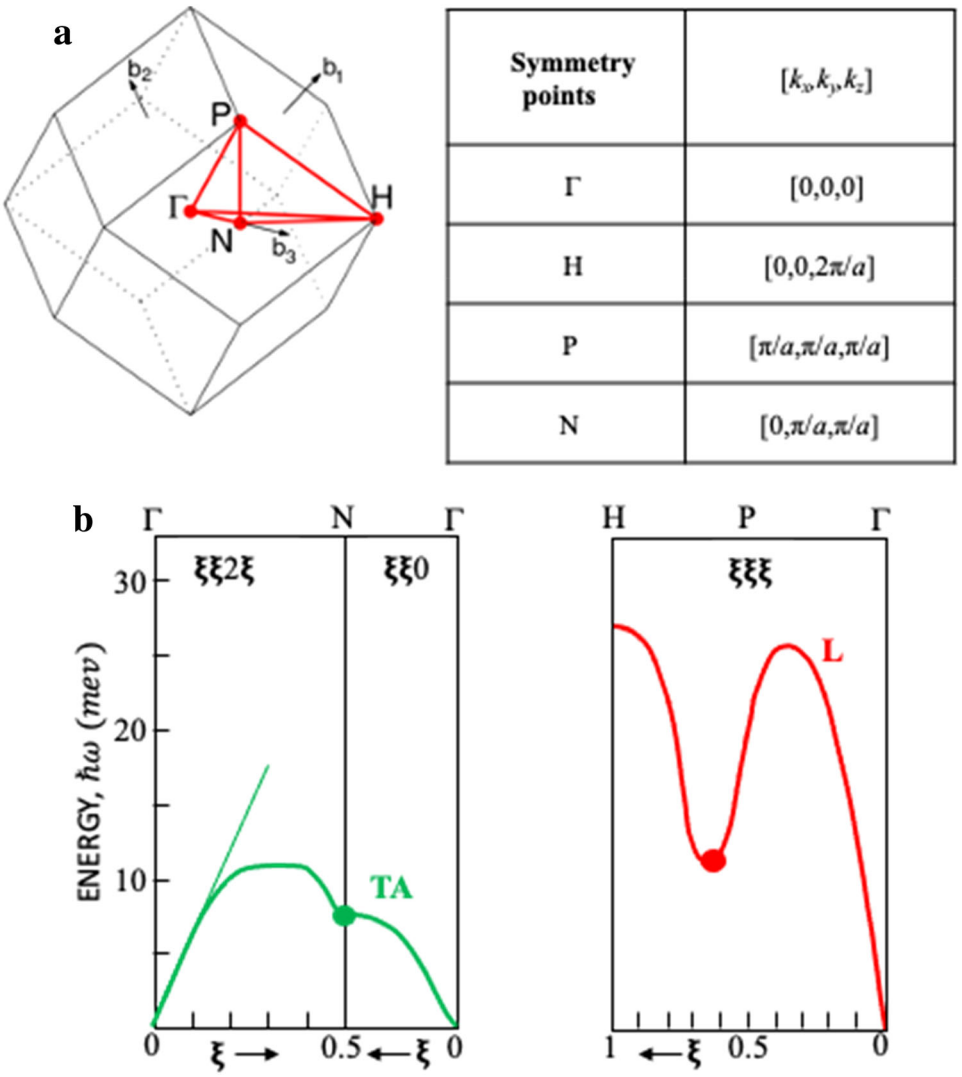

Fig. 17 **a** The first Brillouin zone of the bcc lattice. The b1, b2 and b3 vectors in this figure are defined from the primitive cell of the bcc lattice. The reciprocal lattice indices at high symmetry points are given in the table. The $\xi\xi 2\xi$ direction is an off-symmetry phonon branch. The vector PH lies along the $\xi\xi\xi$ direction. **b** Phonon dispersion curves from bcc Ti, adapted from Petry et al. [23]. Only a longitudinal and one transverse wave is shown to illustrate anomalous softening at wave numbers indicted by the green and red circles corresponding to the $\vec{q} = \frac{1}{2}(110)$, $\vec{p} = [1\bar{1}0]$ and $\vec{q} = \frac{2}{3}(111)$, $\vec{p} = [111]$ phonon, respectively. The tangent marked by the thin green line, that is the initial slope of the $\xi\xi 2\xi$ phonon branch, corresponds to the long-wavelength shear $\{112\} < 111 >$

Table 1 Soft phonon modes and equivalent elastic constants

Transformation	Mode	Phonon	Effective C_{ij}
β to ω	LA	$\vec{q} = \frac{2}{3}(111)$	$\frac{1}{3}(C_{11} + 2C_{12} + 4C_{44})$
		$\vec{p} = [111]$	
β to O′	TA	$\vec{q} = \frac{1}{2}(110)$	$\frac{1}{2}(C_{11} - C_{12})$
		$\vec{p} = [1\bar{1}0]$	
Shear	TA	$\vec{q} = (\bar{1}12)$	$C_s = C' + \frac{1}{2}(C_{44} - C')\sin^2\theta_s$
		$\vec{p} = [111]$	θ_s is an angle from the [001] axis defined by $\theta_s = \sin^{-1}[2(C_{11} + C_{12})/(3C_{11} + 5C_{12} + 2C_{44})]^{1/2}$

$\vec{q}$ is the wave number and $\vec{p}$ indicates the polarization direction

nonlinear superelasticity over a wide range of temperatures. As in the case of the O′ to α″ transformation, the degree of lattice shear within the α″ domains formed by cold rolling can increase during cooling leading to the invar and elinvar effects. Clearly, the density of pre-existing embryos (O′ in this case) for α″ formation or the density of nanodomains of α″ induced by cold work and the stability of these domains offers potential for tuning the invar, elinvar and superelastic effects through compositional control, and offers a fertile field for research should applications emerge. The effect of the combined presence

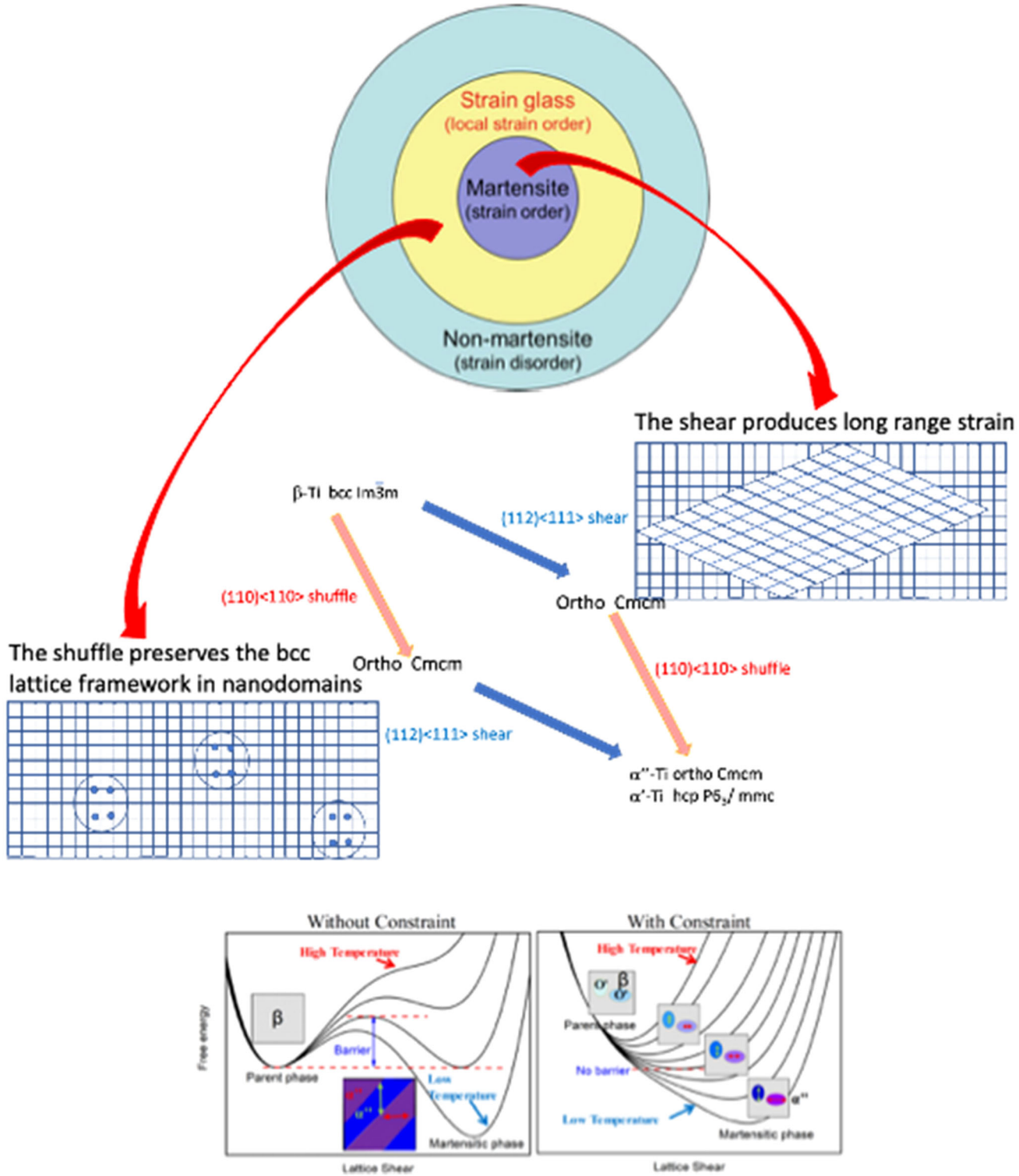

Fig. 18 The O′ phase as a strain glass of nanoembryos for the subsequent shear to martensite, in contrast to the long-range strain state in martensite plates produced when shear precedes the shuffle [26]. The Landau free energy landscape related to transformation to martensite by shear in contrast to transformation to martensite by O″ is also shown [19]

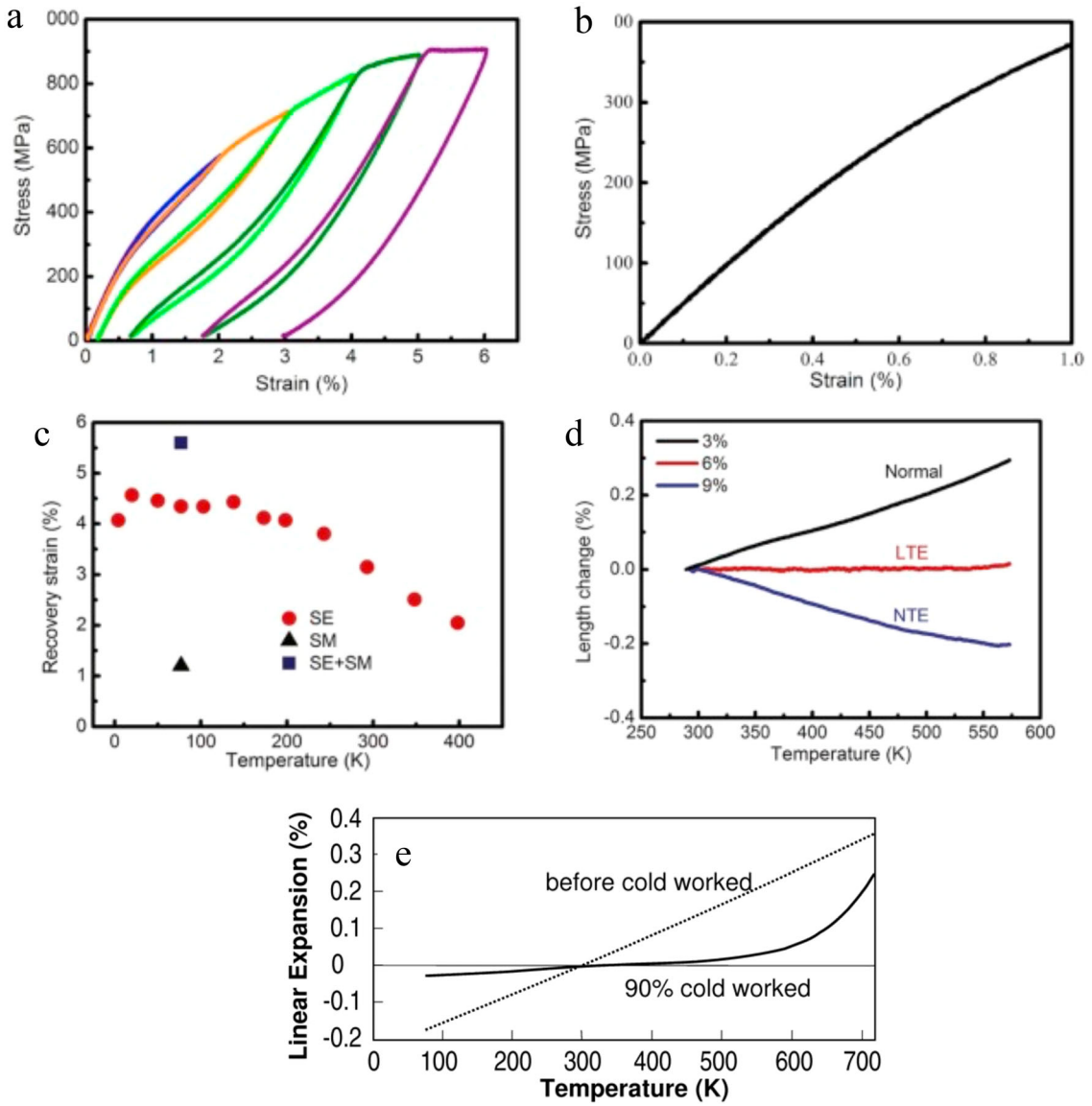

Fig. 19 Multifunctional behaviour associated with nanomartensitic structures; **a** low hysteresis superelasticity in Ti2448 with **b** nonlinear behaviour and **c** the temperature range over which superelasticity is observed **d** CTE can be tuned by applied strain in Ti2448 to invar behaviour (LTE), or negative CTE (NTE) and normal behaviour; **e** elinvar behaviour in gum metal. **a–d** from Hao et al. [29] and **e** from Saito et al. [28]

of O′ and ω phases and the potential increase of ω volume fraction on cooling must also be understood.

5 Summary

The martensitic transformation from the parent β phase in titanium alloys leads to a hexagonal product that transitions to martensite with orthorhombic symmetry with increasing β stabilizer addition. The structural relationship between the parent and product phases is described. The atomic movements leading to the martensite are shown to be accomplished by a long-range shear that transforms the parent to the product lattice and a short-wavelength displacement that induces the correct stacking. The microstructures arising out of these pathways depend on which of these initiates the transformation. Each of these paths is related to softening of specific phonon modes or equivalently softening of related elastic constants with cooling. We show that the nature of alloying affects the sequence of paths. When the short-wavelength displacement or shuffle precedes the shear, the intermediate

product, designated the O′ phase, is present as nanodomains which transform to nanomartensite dispersions on cooling or cold working, resulting in continuous and controlled strain incorporation into the lattice. This transformation mode can lead to low hysteresis, nonlinear superelasticity, and the invar or elinvar effects.

Acknowledgements DB acknowledges the INSA senior scientist fellowship. YW acknowledges financial support from the National Science Foundation, USA, under Grant DMR-1923929. YZ appreciates financial support from National Science Foundation, Grant CMMI-2122272. RB and HLF acknowledge support by the National Science Foundation (NSF), Division of Materials Research (DMR) under Grants DMR-1905844 and DMR-1905835.

References

1. S. Banerjee and P. Mukhopadhyay, Phase Transformations Examples from Titanium and Zirconium Alloys, Elsevier Science, 2007. https://www.sciencedirect.com/bookseries/pergamon-materials-series/vol/12/suppl/C.
2. W.G. Burgers, *Physica*. **1** (1934) 561. https://doi.org/10.1016/S0031-8914(34)80244-3.
3. R. Shi, N. Ma, Y. Wang, *Acta Mater*. **60** (2012) 4172. https://doi.org/10.1016/j.actamat.2012.04.019.
4. M. Abdel-Hady, K. Hinoshita, M. Morinaga, *Scr. Mater.* **55** (2006) 477. https://doi.org/10.1016/j.scriptamat.2006.04.022.
5. Y. Fukui, T. Inamura, H. Hosoda, K. Wakashima, S. Miyazaki, *Mater. Trans*. **45** (2004) 1077. https://doi.org/10.2320/matertrans.45.1077.
6. E. Takahashi, T. Sakurai, S. Watanabe, N. Masahashi, S. Hanada, *Mater. Trans.* **43** (2002) 2978. https://doi.org/10.2320/matertrans.43.2978.
7. S. Miyazaki, H.Y. Kim, H. Hosoda, *Mater. Sci. Eng. A*. **438–440** (2006) 18. https://doi.org/10.1016/j.msea.2006.02.054.
8. R.H. Ericksen, R. Taggart, D.H. Polonis, *Acta Metall.* **17** (1969) 553. https://doi.org/10.1016/0001-6160(69)90114-X.
9. P.M. Hammond and C. Kelly, Martensitic transformations in titanium alloys, in: R.I Jaffee, R.I. and N.E. Promisel (Ed.), Pergamon-Elsevier Science Ltd, (1970) pp. 659 https://doi.org/10.1016/C2013-0-01574-5
10. K.M. Knowles, and D.A. Smith, **Acta Metall. 29** (1981) 1445. https://doi.org/10.1016/0001-6160(81)90179-6.
11. K.M. Knowles, Proceedings of the Royal Society of London. Series A, Mathematical and Published by: Royal Society Stable **380** (1982) 187.
12. D. Banerjee, K. Muraleedharan, J.L. Strudel, *Philos. Mag. A*. **77** (1998) 299. https://doi.org/10.1080/01418619808223754.
13. M. Tahara, H.Y. Kim, T. Inamura, H. Hosoda, S. Miyazaki, *Acta Mater.* **59** (2011) 6208. https://doi.org/10.1016/j.actamat.2011.06.015.
14. Y. Zheng, R.E.A. Williams, S. Nag, R. Banerjee, H.L. Fraser, D. Banerjee, *Scr. Mater.* **116** (2016) 49. https://doi.org/10.1016/j.scriptamat.2016.01.024.
15. Y. Zheng, D. Banerjee, H.L. Fraser, *Scr. Mater.* **116** (2016) 131. https://doi.org/10.1016/j.scriptamat.2016.01.044.
16. Y. Zheng, T. Alam, R. Banerjee, D. Banerjee, H.L. Fraser, *Scr. Mater.* **152** (2018) 150. https://doi.org/10.1016/j.scriptamat.2018.04.030.
17. D. Banerjee, A.K. Gogia, T.K. Nandi, V.A. Joshi, *Acta Metall.* **36** (1988) 871. https://doi.org/10.1016/0001-6160(88)90141-1.
18. Y. Zheng, S. Antonov, Q. Feng, R. Banerjee, D. Banerjee, H.L. Fraser, *Scr. Mater.* **176** (2020) 7. https://doi.org/10.1016/j.scriptamat.2019.09.027.
19. Q. Liang, D. Wang, Y. Zheng, S. Zhao, Y. Gao, Y. Hao, R. Yang, D. Banerjee, H.L. Fraser, Y. Wang, *Acta Mater.* **186** (2020) 415. https://doi.org/10.1016/j.actamat.2019.12.056.
20. N. Nakanishi, A. Nagasawa, Y. Murakami. *J. Phys. Colloques* **43** (1982) C4–35.
21. A. Nagasawa, N. Nakanishi, and K. Enami, Phils. Mag. A **43**, 1345. https://doi.org/10.1080/01418618108239514
22. P.A. Fleury, *Annu. Rev. Mater. Sci*. **6** (1976) 157.
23. W. Petry, M. Alba, *Phys. Rev.* **43** (1991).
24. Y. Hanlumyuang, R.P. Sankaran, M.P. Sherburne, J.W. Morris, D.C. Chrzan, *Phys. Rev. B - Condens. Matter Mater. Phys.* **85** (2012) 1. https://doi.org/10.1103/PhysRevB.85.144108.
25. Y. Ji, S. Ren, D. Wang, Y. Wang, X. Ren, *Springer Ser. Mater. Sci.* **275** (2018) 183. https://doi.org/10.1007/978-3-319-96914-5_7.
26. X. Ren, Phys. *Status Solidi Basic Res*. **251** (2014) 1982. https://doi.org/10.1002/pssb.201451351.
27. J. He, D. Li, W. Jiang, L. Ke, G. Qin, Y. Ye, Q. Qin, D. Qiu, *Materials (Basel)* 12 (2019). https://doi.org/10.3390/ma12020321.
28. T. Saito, T. Furuta, J.H. Hwang, S. Kuramoto, K. Nishino, N. Suzuki, R. Chen, A. Yamada, K. Ito, Y. Seno, T. Nonaka, H. Ikehata, N. Nagasako, C. Iwamoto, Y. Ikuhara, T. Sakuma, *Science* **300** (2003) 464. https://doi.org/10.1126/science.1081957.
29. Y.L. Hao, H.L. Wang, T. Li, J.M. Cairney, A. V. Ceguerra, Y.D. Wang, Y. Wang, D. Wang, E.G. Obbard, S.J. Li, R. Yang, *J. Mater. Sci. Technol.* **32** (2016) 705. https://doi.org/10.1016/j.jmst.2016.06.017.
30. Y. Wang, D. Wang, S. Hou, Y. Wang, X. Ding, S. Ren, X. Ren, *Acta Mater.* **66** (2014) 349. https://doi.org/10.1016/j.actamat.2013.11.022.
31. L. Zhang, D. Wang, X. Ren, Y. Wang, *Sci. Rep.* **5** (2015) 1. https://doi.org/10.1038/srep11477.
32. Y.C. Xu, C. Hu, L. Liu, J. Wang, W.F. Rao, J.W. Morris, A.G. Khachaturyan, *Acta Mater.* **171** (2019) 240. https://doi.org/10.1016/j.actamat.2019.04.027.
33. J. Zhu, Y. Gao, D. Wang, T.Y. Zhang, Y. Wang, *Acta Mater.* **130** (2017) 196. https://doi.org/10.1016/j.actamat.2017.03.042.
34. J. Zhu, D. Wang, Y. Gao, T.Y. Zhang, Y. Wang, *Mater. Today.* **33** (2020) 17. https://doi.org/10.1016/j.mattod.2019.10.003.
35. J. Zhu, H.H. Wu, X.S. Yang, H. Huang, T.Y. Zhang, Y. Wang, S.Q. Shi, *Acta Mater.* **181** (2019) 99. https://doi.org/10.1016/j.actamat.2019.09.044.